PHYSICAL REVIEW B **79**, 195425 (2009)

First-principles study of the interaction and charge transfer between graphene and metals

P. A. Khomyakov,[1] G. Giovannetti,[1,2] P. C. Rusu,[1] G. Brocks,[1] J. van den Brink,[2,3,4] and P. J. Kelly[1]
[1]*Faculty of Science and Technology and MESA+ Institute for Nanotechnology, University of Twente, P.O. Box 217, 7500 AE Enschede, The Netherlands*
[2]*Instituut-Lorentz for Theoretical Physics, Universiteit Leiden, P.O. Box 9506, 2300 RA Leiden, The Netherlands*
[3]*Institute for Molecules and Materials, Radboud Universiteit, Heyendaalseweg 135, 6525 AJ Nijmegen, The Netherlands*
[4]*Department of Physics, Applied Physics, and Stanford Synchrotron Radiation Laboratory, Stanford University, Stanford, California 94305, USA*
(Received 8 February 2009; published 20 May 2009)

Measuring the transport of electrons through a graphene sheet necessarily involves contacting it with metal electrodes. We study the adsorption of graphene on metal substrates using first-principles calculations at the level of density-functional theory. The bonding of graphene to Al, Ag, Cu, Au, and Pt (111) surfaces is so weak that its unique "ultrarelativistic" electronic structure is preserved. The interaction does, however, lead to a charge transfer that shifts the Fermi level by up to 0.5 eV with respect to the conical points. The crossover from *p*-type to *n*-type doping occurs for a metal with a work function ~5.4 eV, a value much larger than the work function of free-standing graphene, 4.5 eV. We develop a simple analytical model that describes the Fermi-level shift in graphene in terms of the metal substrate work function. Graphene interacts with and binds more strongly to Co, Ni, Pd, and Ti. This chemisorption involves hybridization between graphene p_z states and metal *d* states that opens a band gap in graphene, and reduces its work function considerably. The supported graphene is effectively *n*-type doped because in a current-in-plane device geometry the work-function lowering will lead to electrons being transferred to the unsupported part of the graphene sheet.

DOI: 10.1103/PhysRevB.79.195425 PACS number(s): 73.63.−b, 73.20.Hb, 73.40.Ns, 81.05.Uw

I. INTRODUCTION

The history of carbon-based electronics begins with the discovery of fullerenes and carbon nanotubes that are zero and one dimensional, respectively.[1,2] A very important recent development was the preparation of single monolayers of graphite, now more commonly called graphene, on insulating substrates using micromechanical cleavage[3] that has made possible electron-transport experiments on this purely two-dimensional system.[4–9] These transport measurements reveal high charge-carrier mobilities, quantization of the conductivity, and a zero-energy anomaly in the quantum Hall effect, as predicted theoretically.[10–15] The theoretical studies explain these spectacular effects in terms of graphene's unique electronic structure. Although a single graphene sheet is a zero-gap semiconductor with a vanishing density of states at the Fermi energy, it shows metallic behavior due to topological singularities at the *K* points in the Brillouin zone,[10,11] where the conduction and valence bands touch in so-called conical or Dirac points and the dispersion is essentially linear within ±1 eV of the Fermi energy. Its high charge-carrier mobility and peculiar electronic properties have stimulated considerable research into the possibilities of using graphene for electronic and spintronic applications.

Graphene is often treated theoretically as a free-standing two-dimensional sheet. Although this often appears to be a reasonable model for describing observed properties, in many experimental situations there is deviation from this ideal behavior because of physical contact with the environment. This can consist of atomic and molecular impurities in or on the graphene sheet, contact with an insulating substrate, a gate electrode or metallic leads.[5,8,16–20] While the Fermi energy of free-standing graphene coincides with the conical points, adsorption on substrates can alter its electronic properties significantly.[21–32] For example, the weak interaction of graphene adsorbed on the (0001) surface of insulating hexagonal boron nitride is enough to destroy graphene's characteristic conical points and open a band gap of ~50 meV.[27] Even when the interaction is sufficiently weak to leave the conical points essentially unchanged, it can lead to a large shift of the Fermi energy away from the conical points.[27,32]

Since measurement of the electronic transport properties of graphene requires making contacts with metal leads,[5,20,25,26,33–38] it is important to understand such electronic and structural properties as the charge transfer between graphene and the metal substrate, the graphene-metal binding energies, distances, etc. Charge transfer at a metal-graphene interface results in doping of the graphene sheet. Because the sign and the magnitude of the doping depend upon the metal, *p-n* junctions can be realized by attaching electrodes of different metals to graphene.[20,39–46]

There have been numerous theoretical and experimental studies on semiconducting carbon nanotubes contacted to metals such as Al, Au, Pt, Pd, Ca, and Ti.[47–51] Since a graphene sheet can be considered as a carbon nanotube of infinite radius, the chemical interaction between graphene and metal substrates can be expected to be similar to that between metal contacts and nanotubes.

In this paper we use first-principles calculations at the level of density-functional theory (DFT) to characterize the adsorption of graphene on a variety of metal substrates. A preliminary account of our results was given in Ref. 32. The (111) surfaces of Al, Co, Ni, Cu, Pd, Ag, Pt, and Au, and the Ti (0001) surface cover a wide range of work functions and different types of chemical bonding, which allows for a sys-

tematic study of the metal-graphene interface. We focus on the interaction and charge transfer between graphene and the metal substrate, and in particular the effects they have on the doping of graphene by the metal. Because the charge redistribution at the graphene-metal interface can be characterized experimentally by measuring the work function of the graphene-covered metal, we also calculate the work functions of these systems.

The structural details of the metal-graphene interfaces will be presented elsewhere.[52] The most important result for the purposes of this study is that there are two classes of graphene-metal interfaces. Whereas graphene is chemisorbed on Co, Ni, Pd, and Ti, the binding to Al, Cu, Ag, Au, and Pt is much weaker. The electronic structure of graphene is strongly perturbed by chemisorption but is essentially preserved in the weak binding "physisorption" regime. For physisorbed graphene there is generally electron transfer to (from) the metal substrate, causing the Fermi level to move downward (upward) from the graphene conical points. This can be viewed as doping graphene with holes (electrons) by adsorption.

Naively one might expect the type and amount of doping to depend only on the difference between the work functions of free-standing graphene and of the clean metal surface. At typical equilibrium separations, the potential profile and therefore the doping are, however, altered significantly by an interface dipole arising from a direct short-range metal-graphene interaction. Using the DFT results, we develop an analytical model that quantitatively describes the doping of physisorbed graphene. This model also predicts how physisorption of graphene modifies the metal work function.

In order to characterize the doping of chemisorbed graphene a different approach must be used. Since chemisorption perturbs the electronic structure of graphene strongly, doping cannot be simply deduced from the shift of the Fermi level with respect to the conical points. Instead, we consider the work function of the graphene-covered metal, which is always a well-defined quantity. In a current-in-plane (CIP) transport experiment, only part of the graphene sheet covers (or is covered by) the metal electrode, whereas an adjacent part is free standing. The difference between the work function of the graphene-covered metal electrode and free-standing graphene then determines the direction of the charge transfer between these two parts and hence the doping. According to this model, graphene is doped *n*-type by Co, Ni, Pd, and Ti contacts.

The paper is organized as follows. In Sec. II we state the most important computational details of the density-functional calculations and summarize in Sec. III A the key results of a more extensive study of the binding of graphene to various metal substrates.[52] Section III B contains results of the first-principles calculations for the doping and work function of graphene adsorbed on these different substrates. A phenomenological model to describe the doping and work function of physisorbed graphene is introduced in Sec. III C and in Sec. III D chemisorbed graphene is discussed. The sensitivity of the results to the computational approximations used is discussed in Sec. III E. A short discussion and conclusions are presented in Sec. IV.

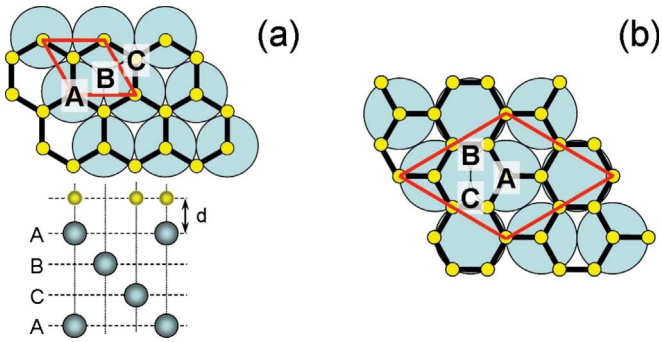

FIG. 1. (Color online) (a) The most stable symmetric configuration of graphene on Cu, Ni, and Co (111) has one carbon atom on top of a metal atom (*A* site), and the second carbon on a hollow site (*C* site). (b) Graphene on Al, Au, Pd, and Pt (111) can be modeled in a 2×2 graphene supercell with eight carbon atoms and three metal atoms per layer. Shown is the most stable symmetric geometry.

II. COMPUTATIONAL DETAILS

We calculate DFT ground-state energies, and optimized geometries using a plane-wave basis set and the PAW formalism at the level of the local (spin) density approximation [L(S)DA],[57] as implemented in the VASP code.[58–61] The plane-wave kinetic-energy cutoff is set at 400 eV. A metal surface is modeled in a supercell as a finite number of layers of metal plus a region of vacuum repeated periodically in the direction perpendicular to the layers. The supercell used to model the graphene-metal adsorption is constructed from a slab of six layers of metal atoms with a graphene sheet adsorbed on one side and a vacuum region of $\sim$12 Å. A dipole correction is applied to avoid spurious interactions between periodic images of the slab.[62]

We choose the in-plane lattice constant of graphene equal to its optimized LDA value, $a=2.445$ Å, adapting the lattice constants of the metals accordingly. The graphene honeycomb lattice then matches the triangular lattice of the metal (111) surfaces in the lateral unit cells shown in Fig. 1. The approximation made by this matching procedure is reasonable since the mismatch with the lattice parameters of the metal (111) surfaces is only 0.8–3.8%, as seen in Table I. In optimizing the geometry, the positions of the carbon atoms as well as those of the top two layers of metal atoms are allowed to relax. All results reported in this paper are obtained for structures adapted to the LDA-optimized in-plane lattice constant of graphene.

We use the tetrahedron scheme[63] for accurate Brillouin zone (BZ) integrations, sampling the BZ of the small and large cells in Fig. 1 with 36×36 and 24×24 **k**-point grids, respectively, and explicitly including the Γ, *K*, and *M* high-symmetry points. Note that on doubling the graphene lattice vectors to match those of Au, Pt, Cu, Ag, Al, and Pd, the *K* point corresponding to the primitive unit cell of graphene is folded down onto the $\bar{K}$ point of the smaller Brillouin zone. The electronic self-consistency criterion is set to 10^{-7} eV. Such a strict convergence is required to obtain accurate forces, which are essential in order to obtain reliable optimized structures. Total energies are converged to within

TABLE I. $a_{\mathrm{hex}}^{\mathrm{exp}}$ and $\tilde{a}_{\mathrm{hex}}^{\mathrm{exp}}$ represent the experimental cell parameters of the surface unit cells shown in Figs. 1(a) and 1(b), respectively, for graphene on various metals. All calculations are performed with the lattice constant of graphene optimized using the LDA, $a_{\mathrm{hex}}=2.445$ Å, except for Ti for which $a_{\mathrm{hex}}=2.46$ Å was used. The calculated equilibrium separation d_{eq} is the separation in the z direction between the carbon atoms of the graphene sheet and the relaxed positions of the topmost metal layer, averaged where applicable over the carbon and metal atoms in the lateral supercell. The binding energy ΔE is the energy per carbon atom required to remove the graphene sheet from the metal surface. W_{M} and W are, respectively, the calculated work functions of the clean metal surfaces, and of free-standing and adsorbed graphene, and $W_{\mathrm{M}}^{\mathrm{exp}}$ and W^{exp} are the corresponding experimental values. ΔE_{F} is the Fermi-level shift of physisorbed graphene.

	Gr	Ti	Ni	Co	Pd	Al	Ag	Cu	Au	Pt
$a_{\mathrm{hex}}^{\mathrm{exp}}$ (Å)	2.46	2.95	2.49	2.51				2.56		
$\tilde{a}_{\mathrm{hex}}^{\mathrm{exp}}$ (Å)	4.92				4.76	4.96	5.00		4.99	4.81
d_{eq} (Å)		2.1	2.05	2.05	2.30	3.41	3.33	3.26	3.31	3.30
ΔE (eV)		0.327	0.125	0.160	0.084	0.027	0.043	0.033	0.030	0.038
W_{M} (eV)		4.56	5.47	5.44	5.67	4.22	4.92	5.22	5.54	6.13
$W_{\mathrm{M}}^{\mathrm{exp}}$ (eV)		4.58[a]	5.35[b]	5.55[c]	5.6[b]	4.24[b]	4.74[b]	4.98[b]	5.31[b]	6.1[d]
W (eV)	4.48	4.17	3.66	3.78	4.03	4.04	4.24	4.40	4.74	4.87
W^{exp} (eV)	4.6[e]		3.9[e]		4.3[e]					4.8[e]
ΔE_{F} (eV)						−0.57	−0.32	−0.17	0.19	0.33

[a]Reference 53.
[b]Reference 54.
[c]Reference 55.
[d]Reference 56.
[e]Reference 21.

10^{-6} eV with respect to ionic relaxation. Explicit total-energy calculations show that the structures in Fig. 1 represent the most stable symmetric configurations of graphene on the metal substrates studied, in agreement with experimental results where available.[21]

Detailed interface structures will be reported elsewhere.[52] Here we note that the L(S)DA functional gives a much better description of graphene-metal substrate binding energies and equilibrium separations than the commonly used generalized gradient approximation (GGA) functionals. Since the work functions, calculated with the L(S)DA, of clean metal surfaces and of those covered with graphene are sufficiently accurate, we use the L(S)DA functional. In Sec. IV we will show that, provided the graphene-metal substrate equilibrium separation is obtained correctly, the charge transfer and consequently the doping of graphene do not depend strongly on the choice of density functional.

Matching the graphene lattice with the Ti (0001) surface is more difficult since there is a lattice mismatch of 20%. To accommodate this mismatch we use a graphene 6×6 lateral supercell with the in-plane lattice constant of graphene equal to its experimental value, $a=2.46$ Å, and a BZ sampling of a similar density as above. The equilibrium separation given in Table I is the value obtained by averaging over the lateral supercell. The details of the graphene/Ti (0001) calculations will be reported elsewhere. Here we focus on the charge redistribution at the interface and the doping of graphene.

III. RESULTS

A. Metal-graphene binding

The calculated equilibrium bonding distances, the binding energies, and the work functions for adsorption of graphene on all metal substrates studied in this paper are listed in Table I. The binding energies ΔE and equilibrium separations d_{eq} immediately show that the metals can be divided into two classes. For graphene adsorbed on Co, Ni, and Pd (111), and Ti (0001), $\Delta E \gtrsim 0.1$ eV/carbon atom and $d_{\mathrm{eq}} \lesssim 2.3$ Å. In contrast, adsorption on Al, Cu, Ag, Au, and Pt (111) leads to much weaker bonding, $\Delta E \lesssim 0.04$ eV/carbon atom, and larger equilibrium separations, $d_{\mathrm{eq}} \sim 3.3$ Å. The equilibrium geometries and separations obtained are in agreement with available experimental data and calculations,[21,23,64,65] and appear to be similar to the bonding found between metals and carbon nanotubes; carbon nanotubes are usually bonded strongly to Pd and Ti, whereas the bonding with Al, Ag, Au, Ca, and Pt is weaker.[47–51]

The difference between the two classes of metal substrates is reflected in the electronic structure of adsorbed graphene as shown in Fig. 2. If the binding energy is large, i.e., if graphene is adsorbed on Co, Ni, Pd, or Ti, the graphene bands are strongly perturbed. In particular, the characteristic conical points of graphene at K are destroyed. Graphene p_z states hybridize (relatively) strongly with the metal d states and the corresponding bands acquire a mixed graphene-metal character. It demonstrates that graphene is chemisorbed on these substrates.

In contrast, if the metal-graphene interaction is weaker, i.e., if graphene is adsorbed on Al, Cu, Ag, Au, or Pt, the graphene bands, including their conical points at K, can still be clearly identified. We reserve the term physisorption to describe this type of bonding. Unlike the case of free-standing graphene where the Fermi level coincides with the conical point, physisorption generally shifts the Fermi level. Even if there is no interaction or the interaction is weak, this does not preclude the transfer of charge between graphene

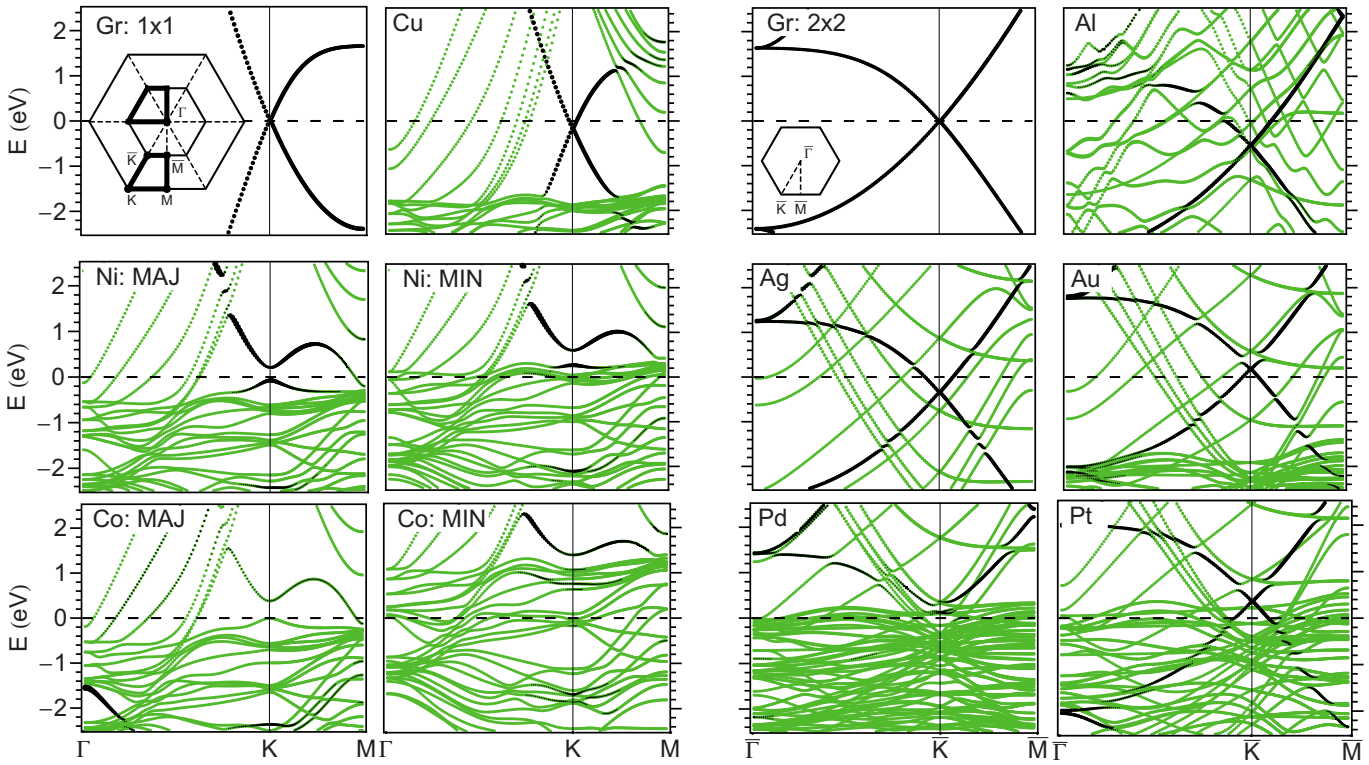

FIG. 2. (Color online) Band structures of graphene adsorbed upon Au, Pt, Cu, Ag, Al, Pd, Ni, and Co (111) substrates. The Fermi level is at zero energy. The amount of carbon p_z character is indicated by the blackness of the bands. The conical point corresponds to the crossing of bands at K with predominantly p_z character, as is clearly visible for (physisorbed) graphene on Au, Pt, Cu, Ag, and Al. For (chemisorbed) graphene on Pd, Ni, and Co, the conical points disappear and the bands have a mixed character. The labels MIN/MAJ indicate the majority- and minority-spin bands of graphene on Ni and Co. The first and third top panels correspond to the band structure of free-standing graphene calculated with the graphene primitive unit cell and 2×2 supercell, respectively. Insets: the two-dimensional Brillouin zones of graphene for the primitive unit cell and 2×2 supercell. In the supercell the bands are downfolded; the area enclosed by the bold lines in the primitive BZ translates to the corresponding one in the supercell BZ.

and the metal substrate resulting from the equilibration of the chemical potentials.

B. Doping of physisorbed graphene

In physisorbed graphene the conical points in the graphene band structure are preserved but charge transfer to or from the metal substrate shifts the Fermi level. A schematic representation of the parameters we use to describe this situation is shown in Fig. 3 for the case of electron transfer from graphene to the metal. A shift upward (downward) with respect to the conical points means that electrons (holes) are donated by the metal to graphene, making the latter n-type (p-type) doped. We extract the Fermi level shifts ΔE_F of graphene physisorbed on a number of metals from the band structures shown in Fig. 2 and plot them in Fig. 4. At equilibrium separations from the metal substrates, graphene is doped n type on Al, Ag, and Cu, and p type on Au and Pt. In the following section we develop a phenomenological model to describe these first-principles results. In the remaining part of this section we identify the physical parameters that play a role in this model.

The work function W of a graphene-covered metal is given by the position of the Fermi level ($W=-E_F$). Because the density of states of graphene is so small compared to that of the density of states of a typical transition-metal surface, the shift required to equilibrate the Fermi levels upon charge transfer takes place almost entirely in graphene. For physisorbed graphene where the interaction is so weak that its

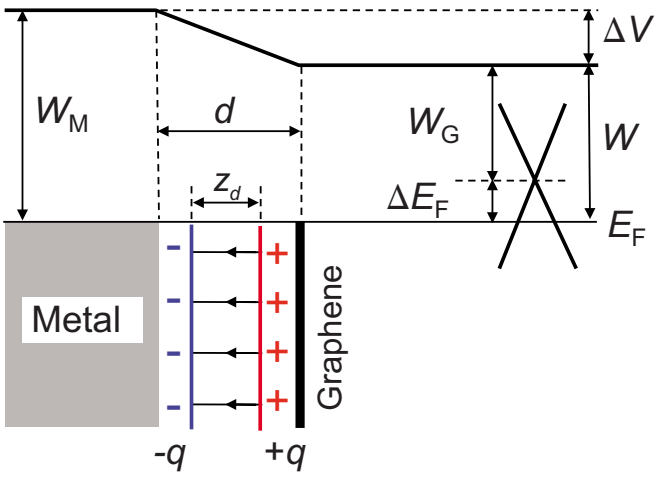

FIG. 3. (Color online) Schematic illustration of the parameters used in modeling the interface dipole and potential step formation at the graphene-metal interface.

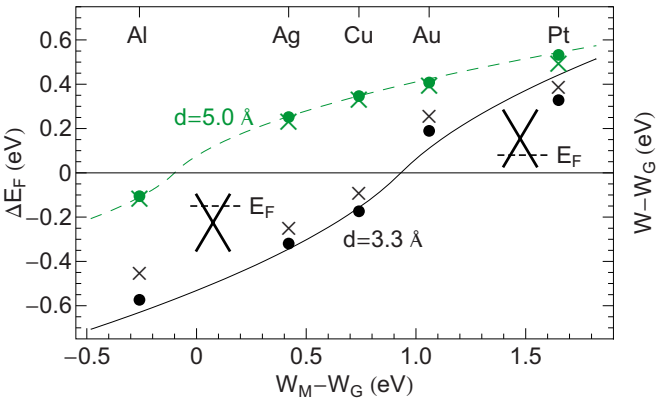

FIG. 4. (Color online) Calculated Fermi energy shift with respect to the conical point, ΔE_F (dots), and $W-W_G$ (crosses) as a function of the clean metal-graphene work-function difference W_M-W_G. The lower (black) and the upper (green/gray) points are for the equilibrium ($d\sim3.3$ Å) and large ($d=5.0$ Å) graphene-metal-surface separations, respectively. The solid and dashed lines follow from the model of Eq. (7) with $d=3.3$ and 5.0 Å, respectively. The insets illustrate the position of the Fermi level with respect to the conical point.

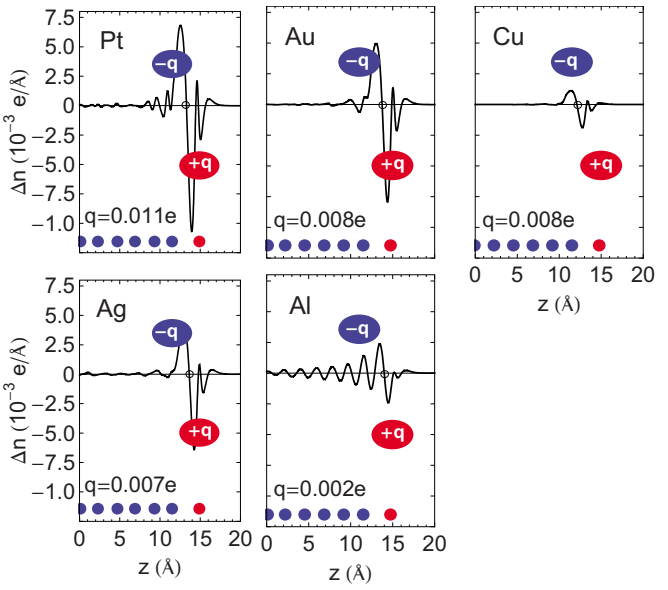

FIG. 5. (Color online) Plane-averaged electron difference density $\Delta n(z)$ (per unit cell) showing the charge displacement upon physisorption of graphene on M (111) surfaces where M=Al, Ag, Cu, Au, and Pt. q/e is the number of electrons per carbon atom calculated by integrating $\Delta n(z)$ from the central node (open black circle) to infinity (Ref. 66).

electronic structure is unchanged, W should be related to the Fermi-level shift in a simple way

$$\Delta E_F = W - W_G, \tag{1}$$

where W_G is the work function of free-standing graphene. The work-function shifts are calculated separately and are plotted in Fig. 4. We see that, while Eq. (1) holds for a relatively large separation $d=5.0$ Å between the graphene sheet and the metal surface, there is a small deviation of ~0.08 eV at the equilibrium separation $d\approx3.3$ Å that can be traced to a perturbation of the graphene electronic structure by physisorption, which cannot be described as a rigid shift. In the following discussions we will neglect this small perturbation. If graphene is chemisorbed and the Fermi-level shift cannot be determined from the strongly perturbed band structure, the work function W is still a well-defined parameter.

Because the work functions of graphene, W_G, and of most metal surfaces, W_M, differ, electrons are transferred from one to the other to equilibrate the Fermi levels if the two systems communicate. Charge transfer between metal and graphene results in the formation of an interface dipole layer and an associated potential step, ΔV. We can use the plane-averaged electron densities $n(z)$ to visualize the electron redistribution upon formation of the interface

$$\Delta n(z) = n_{M|G}(z) - n_M(z) - n_G(z), \tag{2}$$

where $n_{M|G}(z)$, $n_M(z)$, and $n_G(z)$ denote the plane-averaged densities of the graphene-covered metal, the clean metal surface, and free-standing graphene, respectively. Here the structure of the clean metal surface is taken to be the same as that of the graphene-covered metal surface. The results for graphene physisorbed on Al, Cu, Ag, Au, and Pt are shown in Fig. 5. Δn is localized near the interface for all metal substrates and in the majority of cases it has the shape of a simple dipolar charge distribution.

We estimate the charge q (per carbon atom) that is responsible for the dipole by integrating Δn from the node at z_0 between the metal surface and the graphene sheet,

$$q = -e\int_{z_0}^{\infty} dz\Delta n(z)/N_C, \tag{3}$$

where N_C is the number of carbon atoms in the unit cell; $-e$ is the charge of an electron. These numbers are included in Fig. 5. The sign and size of the dipole charges are consistent with the changes in the metal work function upon adsorption of graphene. Note that relatively small values of charge transfer give rise to quite substantial work-function changes, see Table I.

The above analysis points to the use of a plane capacitor model to describe the potential step ΔV. As sketched in Fig. 3, the charge distribution is then modeled as two sheets of charge $\pm q$. Since the charge is predominantly localized between graphene and the metal surface, the effective distance z_d between the charge sheets should be smaller than the graphene-metal separation d.

If the interaction between graphene and the metal surface is weak, as in the case of physisorption, one naively expects that electrons will be transferred to graphene if the clean metal work function is lower than that of free-standing graphene, i.e., if $W_M<W_G$. Electrons should then flow from graphene to the metal surface if $W_M>W_G$ and the crossover point from n- to p-type doping would be exactly at $W_M=W_G$. The results obtained for the equilibrium graphene-metal separation, $d\sim3.3$ Å in Fig. 4, do not confirm this

simple picture of the doping mechanism. Instead, the crossover point between *n*- and *p*-type doping is found for a metal with a work function $W_M = W_G + 0.9$ eV.

This simple picture of charge transfer cannot be entirely wrong. If the graphene-metal separation is increased, the crossover point from *n*- to *p*-type doping decreases to its expected value, $W_M \sim W_G$, for large separations. This is illustrated by the upper curve in Fig. 4 calculated for a graphene-metal separation of $d=5.0$ Å. It clearly indicates that, at the equilibrium separation $d_{eq} \sim 3.3$ Å, the charge reordering at the graphene-metal interface is the result not only of a charge transfer between metal and graphene electronic levels that equilibrates the graphene and metal Fermi energies but that there is also a contribution from a direct interaction between the metal and graphene. A similar interaction, which has a significant repulsive contribution, plays an important role in describing the dipole formation for closed-shell atoms and organic molecules adsorbed upon metal surfaces.[67,68] The interaction depends on the wave function overlap between the metal and the adsorbed species. We expect it therefore to be very sensitive to the metal-graphene separation d and to vanish exponentially with increasing d.

C. Phenomenological model

In this section we construct a simple and general model to describe the Fermi-level and work-function shifts calculated from first-principles for graphene physisorbed on Al, Ag, Cu, Au, and Pt substrates. All relevant parameters are shown in Fig. 3. We start by writing the work function of the graphene-covered metal as $W(d)=W_M-\Delta V(d)$, where ΔV is the potential step generated by the interface dipole layer. Its size depends on the graphene-metal separation d. The Fermi-level shift in graphene and the work function are related by Eq. (1). Use of these relations implicitly assumes that the graphene electronic energy levels around the Fermi energy are essentially unchanged by the interaction between graphene and the metal, and that the band structure of graphene is just rigidly shifted by the interface potential ΔV.

A key element of the model is to write the interface potential step as $\Delta V(d)=\Delta_{tr}(d)+\Delta_c(d)$. The first term, $\Delta_{tr}(d)$, results from the direct charge transfer between graphene and the metal, which is driven by the difference in work functions. The second term, $\Delta_c(d)$, describes the short-range interaction discussed in the previous section, which results from the overlap of the metal and graphene wave functions. We parametrize it as

$$\Delta_c(d) = e^{-\gamma d}(a_0 + a_1 d + a_2 d^2), \tag{4}$$

i.e., we assume that it vanishes exponentially with increasing graphene-metal separation d. The exact asymptotic functional dependence of $\Delta_c(d)$ for large d would very likely change if one were to go beyond DFT and LDA, and take the van der Waals interaction into account. The asymptotic form of $\Delta_c(d)$ is, however, not important because $|\Delta_c(d)|$ becomes negligible for large d anyway.

To model the electron transfer contribution, $\Delta_{tr}(d)$, we use a plane capacitor model so $\Delta_{tr}(d)=\alpha N(d) z_d$, where $\alpha = e^2/\varepsilon_0 A = 34.93$ eV/Å with $A=5.18$ Å^2 as the area of the graphene unit cell, and $N(d)$ is the number of electrons (per unit cell) transferred from graphene to the metal. Note that $N(d)$ becomes negative if electrons are transferred from the metal to graphene. The parameter z_d is the effective distance between the sheets of transferred charge on graphene and the metal. It is smaller than the geometrical metal-graphene separation, $z_d < d$, because most of the charge is localized between the graphene layer and the metal surface. We approximate the effective distance between the charge sheets by $z_d = d - d_0$ with d_0 as a constant.

A closed set of equations for the Fermi-level shift ΔE_F and the work function W is obtained by determining the relation between ΔE_F and the number of electrons N transferred between graphene and the metal. For an energy range within ± 1 eV of the conical points, the graphene density of states is described well by a linear function

$$D(E) = D_0 |E|, \tag{5}$$

with $D_0 = 0.09/(\text{eV}^2$ unit cell). Integrating the density of states from the neutrality point, $\int_0^{\Delta E_F} dE D(E)$, yields the required relation, $N = \text{sign}(\Delta E_F) D_0 \Delta E_F^2 / 2$.[66]

The model can be summarized by the set of equations

$$\begin{aligned} W(d) &= W_M - \Delta V(d), \\ \Delta V(d) &= \Delta_{tr}(d) + \Delta_c(d), \\ \Delta_{tr}(d) &= \alpha N(d)(d - d_0), \\ N(d) &= \text{sign}(\Delta E_F)\frac{1}{2} D_0 \Delta E_F(d)^2, \\ \Delta E_F(d) &= W(d) - W_G. \end{aligned} \tag{6}$$

Solving this set results in the following simple expression for the Fermi-level shift

$$\Delta E_F(d) = \pm \frac{\sqrt{1 + 2\alpha D_0 (d - d_0)|W_M - W_G - \Delta_c(d)|} - 1}{\alpha D_0 (d - d_0)}, \tag{7}$$

where the sign of ΔE_F is determined by the sign of $W_M - W_G - \Delta_c$. The work function of the graphene-covered metal surface is then obtained from Eq. (1).

We used first-principles calculations to obtain ΔE_F and W explicitly for a range of separations d. These first-principles data points are shown in Fig. 6. We could now fit the model to these points and so obtain a simple interpretation of the numerical results. However, we can do better than that. It turns out that the parameter d_0 and the function $\Delta_c(d)$ depend only very weakly on the metal substrate. This means that we can fit these quantities to the first-principles results for a single metal substrate, and subsequently use $\Delta_c(d)$ and d_0 as universal parameters to predict the Fermi-level shifts in graphene for all metal substrates. To determine d_0 and $\Delta_c(d)$ we use the DFT results for graphene on the Cu (111) surface.[69]

The Fermi-level shift for graphene physisorbed on any other metal substrate can then be obtained from the model,

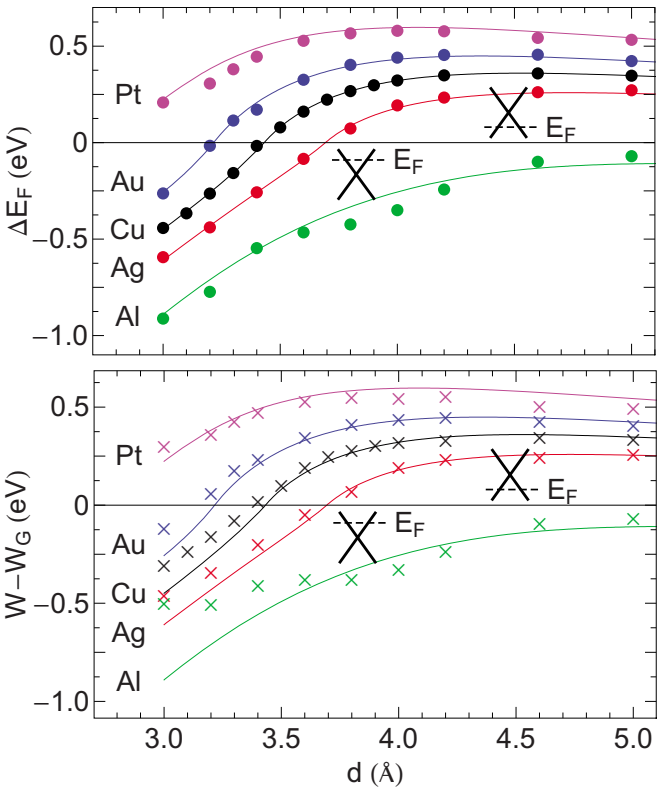

FIG. 6. (Color online) Top panel: Fermi level shifts relative to the Dirac point, $\Delta E_F(d)$, as a function of the grapheme-metal separation d for physisorbed graphene. Bottom panel: calculated work functions $W(d)$ relative to that of a free graphene sheet, W_G. The dots (top) and crosses (bottom) give the calculated DFT-LDA results; the solid lines describe the results obtained from the phenomenological model, Eq. (7) (Ref. 69).

using only the work function of the clean metal surface, W_M, and that of free-standing graphene, W_G, as input parameters in Eq. (7). The accuracy of this model is demonstrated by Fig. 4 and the top panel of Fig. 6. The latter shows that the distance dependence of the Fermi-level shift is represented very well by the model. For graphene on Cu, Ag, and Au (111) the deviations from the first-principles results are $\ll 0.1$ eV, whereas for graphene on Al and Pt (111) they are still $\lesssim 0.1$ eV. The slightly larger deviations for Al and Pt might be related to the greater complexity of the electronic structures of the open p and d shells of Al and Pt, respectively, compounded by the downfolding associated with a larger interface unit cell which makes it more difficult to achieve the same degree of numerical convergence found for Cu, Ag, and Au.

Once ΔE_F has been determined, the work function W of the metal-graphene system can be obtained using Eq. (1) and the results are shown in the bottom panel of Fig. 6. The work function given by the model agrees with the first-principles results within $\lesssim 0.2$ eV for $d \gtrsim 3.3$ Å, the equilibrium separation, but seems to be systematically lower for smaller values of d. The difference becomes smaller upon increasing d. For small graphene-metal separations d, Eq. (1) no longer holds exactly, as the electronic structure of graphene is perturbed by the presence of the metal substrate. Note that, however, 0.2 eV is comparable to the difference between the experimental and the DFT-LDA work functions, see Table I, which means that the error resulting from the model is tolerable.

According to Eq. (6) one can calculate the sign and concentration of the charge carriers in graphene, N, from the Fermi-level shift ΔE_F. The *nominal* charge on graphene per unit cell containing two carbon atoms, eN, is $-14.6e$, $-1.6e$, $-1.3e$, $1.6e$, and $4.9 \times 10^{-3}e$ for graphene on Al, Ag, Cu, Au, and Pt (111), respectively.[66] Although these charges are very small, the Fermi-level shifts are quite substantial because the graphene DOS close to the conical points is so low but they are still within the linear regime described by Eq. (5). In the terminology used in semiconductor physics this amount of charge per unit cell would be classified as heavy doping.

The crossover from p- to n-type doping occurs when the Fermi level coincides exactly with the conical points of graphene, i.e., $\Delta E_F = 0$. According to Eq. (7), this happens if the work function of the metal is given by the critical value

$$W_0(d) = W_G + \Delta_c(d). \tag{8}$$

The critical work function W_0 depends on the graphene-metal separation d since the term Δ_c resulting from the direct graphene-metal interaction depends strongly on d, becoming negligible if $d \gtrsim 4.2$ Å. W_0 then approaches $W_G = 4.5$ eV, i.e., the critical work function is that of free-standing graphene. However, at the equilibrium graphene-metal separation, $d_{eq} = 3.3$ Å, $\Delta_c \approx 0.9$ eV, leading to a critical work function $W_0(d) \approx 5.4$ eV. Although the short-range graphene-metal interaction does not significantly change the graphene band structure, it does lead to a sizeable potential step at the equilibrium separation which is downward from metal to graphene as indicated in Fig. 3. The size of this potential step is relatively insensitive to the metal substrate. A similar potential step has been observed in the adsorption of closed-shell molecules on metal surfaces, where it has been interpreted in terms of an exchange repulsion between the electrons on the molecules and the metal substrate.[68]

The phenomenological model we have outlined describes the doping of graphene by metal contacts and the work-function shifts caused by adsorption of graphene when the graphene-metal bonding is weak. The model is based on the linearity of the graphene DOS, which holds for energies within ± 1 eV around the conical points. Therefore, the criterion for the validity of the model is $\Delta_g \ll |\Delta E_F| \lesssim 1$ eV, where Δ_g is a band gap induced in graphene by interaction with the substrate.[27]

D. Chemisorbed graphene

In the previous sections we defined the doping of physisorbed graphene in terms of the Fermi-level shift ΔE_F with respect to the conical points in the graphene band structure. Negative and positive ΔE_F correspond, respectively, to n-type and p-type dopings. This procedure cannot be used for graphene that is chemisorbed on the Ni, Co, or Pd (111), or on the Ti (0001) surface because the strong graphene-metal bonding interaction destroys the conical points; see the Ni, Co, and Pd panels in Fig. 2.

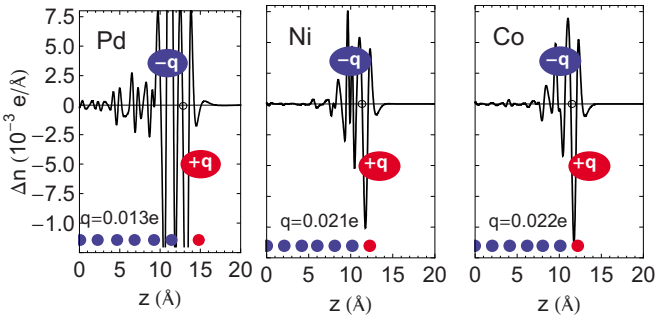

FIG. 7. (Color online) Plane-averaged electron difference density $\Delta n(z)$ (per unit cell) showing the charge displacement upon formation of the chemisorbed graphene-M (111) interface, with M =Ni, Co, and Pd. q is the charge (per carbon atom) calculated by integrating $\Delta n(z)$ from the central nodal point (open black circle) to infinity (Ref. 66).

The more complex bonding of chemisorbed graphene is also illustrated by comparing the plane-averaged electron difference densities $\Delta n(z)$ shown in Figs. 5 and 7. In the physisorption case, Δn still has the characteristics of a simple interface dipole while in the chemisorption case it is much more complicated, indicating the formation of new bonds at the interface between graphene, and Ni, Co, or Pd. The charge reordering at the interface upon chemisorption is substantial, as reflected by the larger values for q given in Fig. 7. This leads to considerable shifts in the metal work functions upon chemisorption of graphene. In all cases studied in this paper graphene acts as an electron donor, lowering the metal work function. For Ni, Co, and Pd (111) the work function lowering is 1.81, 1.66, and 1.64 eV, respectively, and for Ti (0001) it is 0.39 eV.

Despite the impossibility of identifying a Fermi-level shift and therefore the type and magnitude of the doping from a simple examination of the band structures in chemisorbed graphene, it is possible to define a suitable measure for application to CIP geometries. In a CIP geometry only part of the graphene sheet is covered by metal electrodes, and the greater part of the sheet is "free standing." The type and effective concentration of charge carriers in graphene contacted to metallic leads can be measured in experiments using the CIP geometry shown schematically in Fig. 8 (for clarity, for the physisorbed case). At a large distance from the metal contact the Fermi level in free-standing graphene approaches the conical points. At the metallic contact the Fermi level is fixed by the interaction with the metal electrode. The difference between the Fermi levels in adsorbed and free-standing graphene is given by the difference between the work function of the graphene-covered metal surface, W, and that of free-standing graphene, W_G, or in other words, by Eq. (1); see Fig. 8(a). We already used this relation in our description of physisorbed graphene. Since the work function W can be determined for chemisorbed as well as physisorbed graphene, it can be applied to all metal electrodes in the CIP geometry.

To accommodate the Fermi-level difference, charge transfer takes place between the contacted and free-standing regions.[70] Alignment of the Fermi levels results in the band bending shown schematically in Fig. 8(b). The amount of band bending is given by Eq. (1). The band-bending region is p- or n-type doped, depending on the sign of ΔE_F. If $\Delta E_F > 0$, graphene is p-type doped, and if $\Delta E_F < 0$, it is n-type doped. Different metal electrodes can then be used to make p-n junctions in graphene.

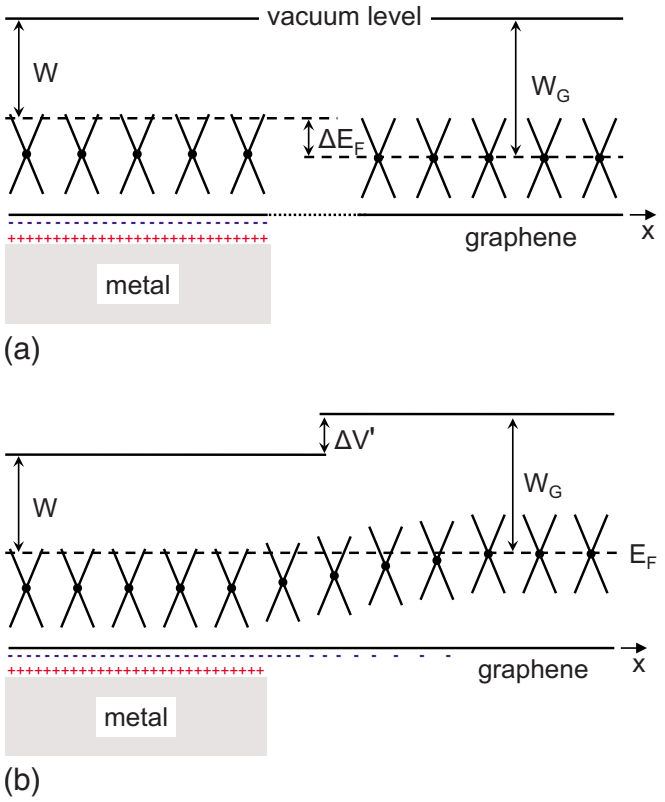

FIG. 8. (Color online) Schematic representation of a graphene sheet partly in contact with a metal electrode. The work function of the graphene-covered metal electrode, W, is here smaller than the work function of graphene, W_G, so that $\Delta E_F < 0$ and the graphene sheet becomes n-type doped. Far from the electrode the conical point of graphene (bold dots) approaches the Fermi energy. (a) In the absence of communication between the graphene-covered metal and the intrinsic graphene sheet, there is a discontinuity ΔE_F of the Fermi energies. (b) As soon as the two systems can communicate, equilibration of the Fermi energies takes place by the transfer of electrons from the low to the high work-function system and the joint Fermi energy is fixed by the graphene-covered metal electrode, $E_F = -W$. This rearrangement of charge gives rise to a potential shift $\Delta V'$. The band bending and graphene doping depend on the distance x from the contact.

For graphene chemisorbed on Ni, Co, Pd (111), and Ti (0001) surfaces, we find $\Delta E_F \equiv W - W_G = -0.82$, -0.70, -0.45, and -0.31 eV, respectively, see Table I. Chemisorption of graphene on these surfaces lowers their work function to below that of free-standing graphene. Therefore, we expect graphene to be n doped by these metal electrodes.

E. Sensitivity to approximations

The calculations on the interaction between graphene and the metal substrates we have discussed so far are at the level of DFT-L(S)DA. The results given in Table I show that cal-

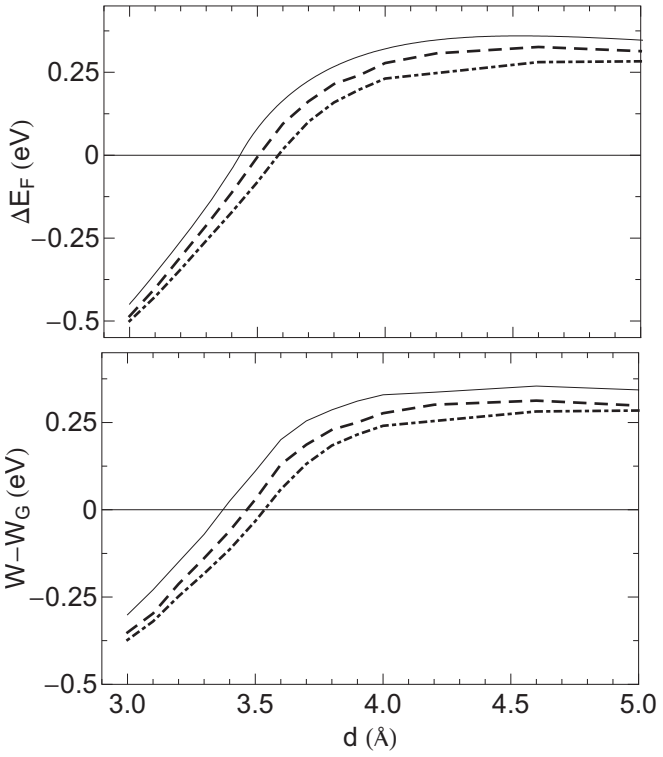

FIG. 9. The dashed lines correspond to the interpolation curves for ΔE_F and $W(d)-W_G$ as a function of the graphene Cu (111)-surface separation d calculated with the PW91 GGA functional. The dash-dotted lines represent the results obtained with the LDA functional with graphene stretched to the Cu (111) lattice constant $a_{hex}=2.49$ Å. As a reference, the solid lines give the LDA results obtained with the optimized graphene lattice constant $a_{hex}=2.445$ Å.

culated work functions of clean metal surfaces agree with experimental data within ~0.2 eV. A similar agreement is observed between calculated work functions of graphene-covered metal surfaces and available experimental data. The change in work function upon graphene adsorption is determined by the formation of an interface dipole and the charge transfer between metal and graphene. Apparently this charge redistribution at the interface is described rather well by the LDA functional.

Semilocal GGA *functionals* are frequently preferred in DFT calculations. For graphene that is physisorbed on a metal surface the commonly used GGA functionals give an interaction that is either too weak or even purely repulsive, making it impossible to predict the equilibrium distance between graphene and the metal surface. In order to test whether the Fermi-level shift in adsorbed graphene and its work function are sensitive to the particular choice of the density functional, we have calculated these parameters for graphene on Cu (111) as a function of the graphene-metal-surface separation, using the PW91 GGA functional.[71,72] The results are shown in Fig. 9. The Fermi-level shifts ΔE_F calculated with GGA are within ~0.07 eV of the ones obtained with LDA. The same holds for the work-function difference $W-W_G$, which means that the description of the doping of graphene is not sensitive to the functional used in the calculations. However, the absolute values of W and W_G calculated using the GGA differ from those obtained using the LDA by ~0.1–0.3 eV, which is a typical difference between work functions obtained with these two density functionals.[68]

Another issue is the possible effect of a truly nonlocal *van der Waals interaction* between the graphene sheet and metal surface, which is neglected in our study. Van der Waals interactions have been addressed recently in calculations on graphite, hexagonal boron-nitride, and diatomic molecules of inert gases.[73,74] A nonlocal correction to a GGA-type density functional has been proposed in Ref. 74 that correctly reproduces the asymptotic van der Waals tail of the binding-energy curve at large intermolecular distances. This nonlocal correction has little impact on the charge distribution, however.[74] Since it is the charge distribution that gives the Fermi-level shift, the work function, and the doping of adsorbed graphene, we conclude that these quantities are adequately described by local or semilocal functionals.

In our calculations we choose the in-plane lattice constant of graphene equal to its optimized LDA value $a=2.445$ Å, and adapt the lattice constants of the metals accordingly. The approximation made by this matching procedure seems reasonable since the mismatch with the lattice parameters of the metal (111) surfaces is only 0.8–3.8%, see Table I. The largest *lattice mismatch* is that between graphene and Cu (111). To estimate the error on the Fermi-level shift and the work function of adsorbed graphene, we have calculated these quantities while stretching graphene to the LDA-optimized in-plane lattice constant of Cu (111) (2.49 Å). The results are shown in Fig. 9. The Fermi-level shifts and work-function differences are within 0.15 eV of the results obtained with the optimized graphene lattice constant. One expects to see a smaller effect for other metals, as the lattice mismatch between graphene and other metals is smaller.

IV. DISCUSSION AND CONCLUSIONS

The theoretical study performed in the previous sections assumes that the graphene sheet is adsorbed on a clean crystalline metal contact. We have used the model represented by Eq. (7) to describe the Fermi-level shift in physisorbed graphene. Interpreting experiments that are not carried out in ultrahigh-vacuum requires some modifications because of impurities that will be present at the metal-graphene interface.[20] The work function of the clean metal surface must then be replaced with that of the metal surface contaminated by water molecules, oxygen, and/or nitrogen, for instance. The short-range graphene-metal-surface interaction, represented by the potential term Δ_c, and the equilibrium separation d_{eq} will also be affected by such adsorbates, and the effects will depend critically upon the adsorbate concentration. The same obviously holds for chemisorbed graphene. A large concentration of adsorbates on the metal surface could break the chemical interaction between graphene and the metal.

In some experiments the interface between the graphene sheet and metal surface might contain a thicker buffer layer consisting, for example, of water, or a metal oxide,[20] which

would certainly modify the graphene-substrate interaction. An input parameter to the model of Eq. (7) then is the work function of the metal with the buffer layer on top. Using the plane capacitor model one should replace α in Eq. (7) by α/κ, where κ is the effective dielectric constant of the buffer layer. Obviously the distance z_d between the charge sheets has to be modified accordingly to take the thickness of the buffer layer into account. In addition, the potential term Δ_c which represents the short-range interaction of graphene with the substrate should now reflect the graphene buffer layer interaction.

A metallic buffer layer consisting of, for instance, Ti is often used in experiments to establish a good contact between graphene and the electrodes. Such layers have a thickness of typically ~ 5 nm, which is sufficiently thick that the contact should be considered as a graphene-Ti contact.

Using first-principles DFT calculations, we have systematically studied the interaction and charge transfer between graphene and a range of metal surfaces with different work functions. We found that graphene is chemisorbed on Co, Ni, and Pd (111) surfaces, and on the Ti (0001) surface and that this strong interaction perturbs the electronic structure of graphene significantly. In contrast, adsorption of graphene on Al, Cu, Ag, Au, and Pt (111) surfaces leads to weak bonding, which preserves the typical graphene electronic structure, including the conical points. Even in this physisorbed case, however, there is a short-range graphene-metal interaction, as well as a charge transfer between the graphene and metal states. These result in a doping of graphene, i.e., a shift of the Fermi level with respect to the conical points, and a significant change in the work function of the graphene-covered metal surfaces, as compared to the clean metal surface.

To extend the applicability of the DFT results on physisorbed graphene we developed a simple general model, which takes into account the charge transfer between the graphene and metal states, and the short-range graphene-metal interaction. We find that the latter only weakly depends on the metal. Therefore it can be fitted using the DFT results on one metal substrate. The model then only has the work functions of free-standing graphene and that of the clean metal surface as input parameters, and it predicts the Fermi-level shift and carrier concentration in graphene, as well as the work function of the graphene-covered metal substrate. We find that graphene is *n*-type doped if the metal work function $W_M \lesssim 5.4$ eV, whereas it is *p*-type doped if $W_M \gtrsim 5.4$ eV.

For the CIP geometry, where only part of the graphene sheet covers the metal electrode, we propose a definition of the doping that is based upon the work function of graphene-covered metal surface. This definition is valid both for the chemisorbed and physisorbed cases. It predicts that adsorption of graphene on Al, Ag, Cu, Co, Ni, and Pd (111) surfaces, and on the Ti (0001) surface leads to *n*-type doping. The high values of the work functions of Au and Pt (111) substrates lead to *p*-type doping of graphene.

Both the analytical model and the CIP definition of the graphene doping are derived from general principles, and should be applicable to any metal surface on which graphene can be epitaxially grown. This opens up the possibility of a general understanding of *p*-*n* junctions prepared by doping graphene with metal contacts.[75]

ACKNOWLEDGMENTS

This work is part of the research programs of "Chemische Wetenschappen (CW)" and the "Stichting voor Fundamenteel Onderzoek der Materie (FOM)," both financially supported by the "Nederlandse Organisatie voor Wetenschappelijk Onderzoek (NWO)," and of "NanoNed," a nanotechnology program of the Dutch Ministry of Economic Affairs. Part of the calculations was performed with a grant of computer time from the "Stichting Nationale Computerfaciliteiten (NCF)."

[1] H. W. Kroto, J. R. Heath, S. C. O'Brien, R. F. Curl, and R. E. Smalley, Nature (London) **318**, 162 (1985).
[2] S. Iijima, Nature (London) **354**, 56 (1991).
[3] K. S. Novoselov, D. Jiang, F. Schedin, T. J. Booth, V. V. Khotkevich, S. V. Morozov, and A. K. Geim, Proc. Natl. Acad. Sci. U.S.A. **102**, 10451 (2005).
[4] K. S. Novoselov, A. K. Geim, S. V. Morozov, D. Jiang, Y. Zhang, S. V. Dubonos, I. V. Grigorieva, and A. A. Firsov, Science **306**, 666 (2004).
[5] K. S. Novoselov, A. K. Geim, S. V. Morozov, D. Jiang, M. I. Katsnelson, I. V. Grigorieva, S. V. Dubonos, and A. A. Firsov, Nature (London) **438**, 197 (2005).
[6] Y. B. Zhang, Y. W. Tan, H. L. Stormer, and P. Kim, Nature (London) **438**, 201 (2005).
[7] S. Y. Zhou, G. H. Gweon, J. Graf, A. V. Fedorov, C. D. Spataru, R. D. Diehl, Y. Kopelevich, D. H. Lee, S. G. Louie, and A. Lanzara, Nat. Phys. **2**, 595 (2006).
[8] K. I. Bolotin, K. J. Sikes, Z. Jiang, G. Fudenberg, J. Hone, P. Kim, and H. L. Stormer, Solid State Commun. **146**, 351 (2008).
[9] R. Danneau, F. Wu, M. F. Craciun, S. Russo, M. Y. Tomi, J. Salmilehto, A. F. Morpurgo, and P. J. Hakonen, Phys. Rev. Lett. **100**, 196802 (2008).
[10] N. H. Shon and T. Ando, J. Phys. Soc. Jpn. **67**, 2421 (1998).
[11] T. Ando, Y. Zheng, and H. Suzuura, J. Phys. Soc. Jpn. **71**, 1318 (2002).
[12] N. M. R. Peres, F. Guinea, and A. H. Castro Neto, Phys. Rev. B **73**, 125411 (2006).
[13] V. P. Gusynin and S. G. Sharapov, Phys. Rev. Lett. **95**, 146801 (2005).
[14] M. I. Katsnelson, K. S. Novoselov, and A. K. Geim, Nat. Phys. **2**, 620 (2006).
[15] J. van den Brink, Nat. Nanotechnol. **2**, 199 (2007).
[16] J. Sabio, C. Seoanez, S. Fratini, F. Guinea, A. H. Castro Neto, and F. Sols, Phys. Rev. B **77**, 195409 (2008).
[17] K. T. Chan, J. B. Neaton, and M. L. Cohen, Phys. Rev. B **77**, 235430 (2008).
[18] O. Leenaerts, B. Partoens, and F. M. Peeters, Phys. Rev. B **77**, 125416 (2008).

[19] D. W. Boukhvalov, M. I. Katsnelson, and A. I. Lichtenstein, Phys. Rev. B **77**, 035427 (2008).
[20] E. J. H. Lee, K. Balasubramanian, R. T. Weitz, M. Burghard, and K. Kern, Nat. Nanotechnol. **3**, 486 (2008).
[21] C. Oshima and A. Nagashima, J. Phys.: Condens. Matter **9**, 1 (1997).
[22] Y. S. Dedkov, A. M. Shikin, V. K. Adamchuk, S. L. Molodtsov, C. Laubschat, A. Bauer, and G. Kaindl, Phys. Rev. B **64**, 035405 (2001).
[23] G. Bertoni, L. Calmels, A. Altibelli, and V. Serin, Phys. Rev. B **71**, 075402 (2005).
[24] A. T. N'Diaye, S. Bleikamp, P. J. Feibelman, and T. Michely, Phys. Rev. Lett. **97**, 215501 (2006).
[25] V. M. Karpan, G. Giovannetti, P. A. Khomyakov, M. Talanana, A. A. Starikov, M. Zwierzycki, J. van den Brink, G. Brocks, and P. J. Kelly, Phys. Rev. Lett. **99**, 176602 (2007).
[26] V. M. Karpan, P. A. Khomyakov, A. A. Starikov, G. Giovannetti, M. Zwierzycki, M. Talanana, G. Brocks, J. van den Brink, and P. J. Kelly, Phys. Rev. B **78**, 195419 (2008).
[27] G. Giovannetti, P. A. Khomyakov, G. Brocks, P. J. Kelly, and J. van den Brink, Phys. Rev. B **76**, 073103 (2007).
[28] S. Marchini, S. Gunther, and J. Wintterlin, Phys. Rev. B **76**, 075429 (2007).
[29] B. Uchoa, C.-Y. Lin, and A. H. Castro Neto, Phys. Rev. B **77**, 035420 (2008).
[30] E. Rotenberg, A. Bostwick, T. Ohta, J. L. McChesney, T. Seyller, and K. Horn, Nature Mater. **7**, 258 (2008).
[31] X. S. Wu, M. Sprinkle, X. B. Li, F. Ming, C. Berger, and W. A. de Heer, Phys. Rev. Lett. **101**, 026801 (2008).
[32] G. Giovannetti, P. A. Khomyakov, G. Brocks, V. M. Karpan, J. van den Brink, and P. J. Kelly, Phys. Rev. Lett. **101**, 026803 (2008).
[33] H. Schomerus, Phys. Rev. B **76**, 045433 (2007).
[34] Y. M. Blanter and I. Martin, Phys. Rev. B **76**, 155433 (2007).
[35] B. Huard, N. Stander, J. A. Sulpizio, and D. Goldhaber-Gordon, Phys. Rev. B **78**, 121402(R) (2008).
[36] R. Nouchi, M. Shiraishi, and Y. Suzuki, Appl. Phys. Lett. **93**, 152104 (2008).
[37] A. J. M. Giesbers, G. Rietveld, E. Houtzager, U. Zeitler, R. Yang, K. S. Novoselov, A. K. Geim, and J. C. Maan, Appl. Phys. Lett. **93**, 222109 (2008).
[38] S. Russo, M. F. Craciun, M. Yamamoto, A. F. Morpurgo, and S. Tarucha, arXiv:0901.0485 (unpublished).
[39] V. V. Cheianov and V. I. Falko, Phys. Rev. B **74**, 041403(R) (2006).
[40] B. Huard, J. A. Sulpizio, N. Stander, K. Todd, B. Yang, and D. Goldhaber-Gordon, Phys. Rev. Lett. **98**, 236803 (2007).
[41] B. Özyilmaz, P. Jarillo-Herrero, D. Efetov, D. A. Abanin, L. S. Levitov, and P. Kim, Phys. Rev. Lett. **99**, 166804 (2007).
[42] J. R. Williams, L. DiCarlo, and C. M. Marcus, Science **317**, 638 (2007).
[43] J. Tworzydlo, I. Snyman, A. R. Akhmerov, and C. W. J. Beenakker, Phys. Rev. B **76**, 035411 (2007).
[44] M. M. Fogler, D. S. Novikov, L. I. Glazman, and B. I. Shklovskii, Phys. Rev. B **77**, 075420 (2008).
[45] C.-H. Park, L. Yang, Y.-W. So, M. L. Cohen, and S. G. Louie, Nat. Phys. **4**, 213 (2008).
[46] R. V. Gorbachev, A. S. Mayorov, A. K. Savchenko, D. W. Horsell, and F. Guinea, Nano Lett. **8**, 1995 (2008).
[47] S. Okada and A. Oshiyama, Phys. Rev. Lett. **95**, 206804 (2005).
[48] Y. Nosho, Y. Ohno, S. Kishimoto, and T. Mizutani, Appl. Phys. Lett. **86**, 073105 (2005).
[49] W. Zhu and E. Kaxiras, Appl. Phys. Lett. **89**, 243107 (2006).
[50] T. Z. Meng, C.-Y. Wang, and S.-Y. Wang, J. Appl. Phys. **102**, 013709 (2007).
[51] V. Vitale, A. Curioni, and W. Andreoni, J. Am. Chem. Soc. **130**, 5848 (2008).
[52] P. A. Khomyakov, G. Giovannetti, P. C. Rusu, G. Brocks, J. van den Brink, and P. J. Kelly (unpublished).
[53] B. T. Jonker, J. F. Morar, and R. L. Park, Phys. Rev. B **24**, 2951 (1981).
[54] H. B. Michaelson, J. Appl. Phys. **48**, 4729 (1977).
[55] T. Vaara, J. Vaari, and J. Lahtinen, Surf. Sci. **395**, 88 (1998).
[56] G. N. Derry and Zhang Ji-Zhong, Phys. Rev. B **39**, 1940 (1989).
[57] J. P. Perdew and A. Zunger, Phys. Rev. B **23**, 5048 (1981).
[58] P. E. Blöchl, Phys. Rev. B **50**, 17953 (1994).
[59] G. Kresse and D. Joubert, Phys. Rev. B **59**, 1758 (1999).
[60] G. Kresse and J. Hafner, Phys. Rev. B **47**, 558 (1993).
[61] G. Kresse and J. Furthmuller, Phys. Rev. B **54**, 11169 (1996).
[62] J. Neugebauer and M. Scheffler, Phys. Rev. B **46**, 16067 (1992).
[63] P. E. Blöchl, O. Jepsen, and O. K. Andersen, Phys. Rev. B **49**, 16223 (1994).
[64] Y. Gamo, A. Nagashima, M. Wakabayashi, M. Terai, and C. Oshima, Surf. Sci. **374**, 61 (1997).
[65] Y. Qi, L. G. Hector, Jr., N. Ooi, and J. B. Adams, Surf. Sci. **581**, 155 (2005).
[66] The definition of q in Eq. (3) is somewhat arbitrary since $\Delta n(z)$ is a continuous function. It is used here only as an estimate for the interface dipole charge and q should not be confused with the charge eN transferred between the graphene sheet and the metal surface which is uniquely defined in terms of ΔE_F. For the metal surfaces studied in this paper, q is positive for equilibrium separations, which leads to a decrease in the work function as compared to the clean metal surface. In contrast, eN, which determines the type of doping of graphene, can be both positive and negative. The two charges, q and eN, are related via Eq. (6) since $eN \propto \Delta E_F$ and $q \propto \Delta V$. One has $q = eN/N_C$ only if $\Delta_c(d) = 0$, which holds if $d \gg d_{eq}$, i.e., if the graphene sheet is far from the metal surface.
[67] J. L. F. Da Silva, C. Stampfl, and M. Scheffler, Phys. Rev. Lett. **90**, 066104 (2003).
[68] P. C. Rusu, Ph.D. thesis, University of Twente, 2007; http://purl.org/utwente/58034
[69] We obtain $\Delta_c(d)$ by least-squares fitting Eq. (7) to the DFT and LDA results for $\Delta E_F(d)$ for Cu (111) with $d_0 = 2.4$ Å. This value of d_0 provides the best fit of $\Delta E_F(d)$. At large d the chemical interaction term $\Delta_c(d)$ should vanish. Parametrizing $\Delta_c(d) = e^{-\gamma d}(a_0 + a_1 d + a_2 d^2)$ yields $\gamma = 1.6443$ Å^{-1}, $a_0 = -2048.56$ eV, $a_1 = 1363.87$ eV/Å, and $a_2 = -205.737$ eV/Å^2, where points with $d \gtrsim 3.0$ Å have been used for the fit. The general applicability of this equation to all metal substrates can be explained in terms of the weak metal-graphene interaction. The electron redistribution is then dominated by exchange repulsion and is almost independent of the metal species (Ref. 68).
[70] The situation is analogous to what happens at the boundary between different facets of a metal crystal when the work function depends on the facet orientation. As a result of the difference in work functions, a transient electron current must flow from the lower work function to the higher work-function surface. This charge rearrangement gives rise to a nonvanishing electrostatic

potential field in the region of the boundary between the different surfaces so that there is no longer a well-defined vacuum level.

[71] J. P. Perdew, J. A. Chevary, S. H. Vosko, K. A. Jackson, M. R. Pederson, D. J. Singh, and C. Fiolhais, Phys. Rev. B **46**, 6671 (1992).

[72] J. P. Perdew, J. A. Chevary, S. H. Vosko, K. A. Jackson, M. R. Pederson, D. J. Singh, and C. Fiolhais, Phys. Rev. B **48**, 4978 (1993).

[73] H. Rydberg, M. Dion, N. Jacobson, E. Schroder, P. Hyldgaard, S. I. Simak, D. C. Langreth, and B. I. Lundqvist, Phys. Rev. Lett. **91**, 126402 (2003).

[74] T. Thonhauser, V. R. Cooper, S. Li, A. Puzder, P. Hyldgaard, and D. C. Langreth, Phys. Rev. B **76**, 125112 (2007).

[75] P. A. Khomyakov, A. A. Starikov, G. Brocks, and P. J. Kelly (unpublished).